Complex dynamics of a single neuron model

S. Popovych,[1] A. Gail,[1] and J. Schropp[1,2]
[1]*Mathematical Institute of the University of Cologne, Cologne, Germany*
[2]*Department of Mathematics and Statistics, University of Konstanz, Konstanz, Germany*
(Received 2 February 2005; revised manuscript received 12 May 2006; published 25 October 2006)

We study a mathematical model of a single neuron with self-coupling. The model is based on the FitzHugh-Nagumo oscillator and an equation describing synaptic properties of the neuron. The analysis of the model is focused on its dynamics, depending on parameters characterizing synaptic time constants and external signals that affect the neuron. Applying Lyapunov exponents and bifurcation analysis, we point out the occurrence of parameter regions with different behavior such as bursting (chaotic or periodic), spiking, and multistable phenomena. Moreover, we can describe the dynamics of the model using an analytical approximation of the one-dimensional Poincaré map extracted from the numerical simulations.

DOI: 10.1103/PhysRevE.74.041914 PACS number(s): 87.19.La, 87.10.+e, 05.45.−a, 02.60.Cb

I. INTRODUCTION

The transmission of information in the brain is accomplished by trains of pulses or action potentials that are often organized in sequences of bursts. Mathematically, the generation of action potentials was first described successfully by Hodgkin and Huxley [1]. The Hodgkin-Huxley model was developed in order to describe the behavior of the nerve cells of the squid giant axon, taking into account different ion channels of the nerve membrane.

The Hodgkin-Huxley system is regarded as a base model for excitable nerve cells. Since the Hodgkin-Huxley system generates only spike oscillations (repetitive firing of the cell) it has to be extended in order to describe bursting of neurons (bursts of oscillatory activity that are interspersed by quasistationary states).

The mathematical modeling of bursting needs a second, slow time scale in addition to the fast time scale that is provided, for example, by the Hodgkin-Huxley model. The slow time scale variable describes usually a nonmembrane quantity, e.g., the total postsynaptic potential of a neuron [2] or the intracellular free calcium concentration in the Chay-Keizer model of pancreatic β cells [3].

Bursting in the context of slow-fast systems has been examined, e.g., by Rinzel [4]. Rinzel describes the generation of bursting due to the interaction of slow and fast times scales in general and for special systems like the Chay-Keizer model and the FitzHugh-Rinzel model for nerve cells. The last model contains the FitzHugh-Nagumo system, which is a simplification of the Hodgkin-Huxley equations [5–7] that describes qualitatively the generation of action potentials at the axon initial segment of the neuron. Such types of neuronal oscillators have been considered, for example, by Plant [8]. There, a mathematical model based on the FitzHugh-Nagumo system was developed in order to investigate the behavior of a single neuron with recurrent activity. Finally, bifurcation sequences that lead to bursting were classified and analyzed in the papers of Izhikevich [9,10].

The mathematical neuron model investigated in the present paper uses a variant of the FitzHugh-Nagumo system to model the action potential generation at the axon initial segment of a neuron. Similar to other nonlinear oscillators used in neuron modeling, the FitzHugh-Nagumo system displays stationary solutions and periodic oscillations depending on the actual value of the bifurcation parameters. The incoming signal of a neuron is described by an additional equation, called network equation that sums up all signals arriving from other connected neurons. The network equation can take into account possible time delays due to signal propagation along the axon, dendrites, and the synapses as well as the strength of the synaptic coupling and time constants of the synapse. The combination of the fast FitzHugh-Nagumo subsystem and the slow network equation results in a nonlinear system of three coupled ordinary or delay differential equations for a single neuron. This system is able to display the two main types of neuronal oscillations that are bursting and spiking. For detailed analytical and numerical investigations of the system, we refer to [2,11].

We study the properties of a single self-coupled neuron model. This case results from a synchronized neural network. It can be shown that under some conditions on the parameters the dynamics of the whole synchronized neural network can be reduced by a homogeneity approach to the dynamics of a single self-coupled neuron [2,12]. Synchronized states in neuronal networks are found, for example, as pathological states in the case of epileptic seizures or Parkinson's disease.

Of particular interest for a better understanding of the model mechanism is the question of whether an explicit delay in the signal propagation is an essential model ingredient to generate the highly appreciated nonlinear solutions like spiking and bursting. From the biological point of view this delay seems to be natural. In special situations (see, e.g., [4]) there are nerve models displaying burst solutions only by the interaction of slow and fast time scales. So here we go along the way of Rinzel [4] and analyze the properties of a single neuron model without retarded signal propagation. We investigate the resulting model dynamics using analytical and numerical approaches. In addition, periodic solutions of the neuron system were characterized with regard to its stability and its transitions to chaotic states.

We show how complex oscillatory dynamics arises in our model depending on the bifurcation parameters. Together with the analysis of the stability of these different states we

obtain a better understanding of the phenomena that can occur in neural networks.

The paper is organized as follows. In Sec. II the mathematical model is introduced and important properties of the system are assorted. Section III gives an overview of the numerically computed dynamical properties of the system for different bifurcation parameters and its stability. In Sec. IV a piecewise monotone one-dimensional Poincaré map is derived from the system in order to obtain a deeper understanding of the dynamics of the system. A discussion of the results in Sec. V concludes the paper.

II. THE MATHEMATICAL MODEL

As explained in the Introduction, we investigate the properties of the core system

$$\tau\dot{U}(t) = -U(t) + qG(V(t)) + e,$$

$$\dot{V}(t) = c\left(W(t) + V(t) - \frac{1}{3}V^3(t)\right) + \gamma U(t),$$

$$\dot{W}(t) = [a - V(t) - bW(t)]/c. \tag{1}$$

In this model the total postsynaptic potential $U(t)$ is generated by the network equation (first equation in the system) that contains the incoming signal and the synaptic properties. Further components of the network equation are the neuronal transfer function

$$G(V) = \frac{1}{1 + \exp(-4V)},$$

which models the relation between the incoming presynaptic potential $V(t)$ and the postsynaptic potential $U(t)$ that is obtained as an answer of the synapse to the incoming signal. The parameter q denotes the synaptic coupling strength. Positive values of q correspond to excitatory synapses, whereas negative q describe inhibitory synapses. The time constant τ characterizes the dynamical properties of the synapse and e considers further external incoming signals. The axon initial segment of the neuron where the outgoing signal $V(t)$ (also called membrane potential) is generated is modeled by the FitzHugh-Nagumo oscillator [(V,W)-subsystem]. The parameter γ couples the total postsynaptic potential $U(t)$ to the axon initial segment. $W(t)$ is an auxiliary variable and a, b, c are parameters of the FitzHugh-Nagumo subsystem.

A. Limit cases

For $\tau \neq 0$ our system (1) can be rewritten in the form

$$\dot{U}(t) = \frac{1}{\tau}[-U(t) + qG(V(t)) + e],$$

$$\dot{V}(t) = c\left(W(t) + V(t) - \frac{1}{3}V^3(t)\right) + \gamma U(t),$$

$$\dot{W}(t) = [a - V(t) - bW(t)]/c. \tag{2}$$

In the case $\tau \gg 1$ the variable U is commonly referred to as the slow variable and V and W are called fast variables. Rescaling the time $s = t/\tau$ gives then a system of the form

$$\dot{U}(t) = -U(t) + qG(V(t)) + e,$$

$$\frac{1}{\tau}\dot{V}(t) = c\left(W(t) + V(t) - \frac{1}{3}V^3(t)\right) + \gamma U(t),$$

$$\frac{1}{\tau}\dot{W}(t) = [a - V(t) - bW(t)]/c. \tag{3}$$

The essential idea in singular perturbation theory is to deduce the behavior of the solutions of the singularly perturbed system by studying the two limiting cases resulting from Eqs. (2) and (3).

The first limit case [$\tau = \infty$ in (2)] defines the fast subsystem

$$\dot{U}(t) = 0,$$

$$\dot{V}(t) = c\left(W(t) + V(t) - \frac{1}{3}V^3(t)\right) + \gamma U(t),$$

$$\dot{W}(t) = [a - V(t) - bW(t)]/c. \tag{4}$$

Equation (4) is a modified FitzHugh-Nagumo system with U being a parameter. In the following we refer to equation (5) when we mention the FitzHugh-Nagumo system

$$\dot{V}(t) = c\left(W(t) + V(t) - \frac{1}{3}V^3(t)\right) + \gamma U,$$

$$\dot{W}(t) = [a - V(t) - bW(t)]/c. \tag{5}$$

System (5) has been investigated intensively [4,11,16–18]. We summarize some important previous results that are valid for parameter ranges that correspond to interesting neural dynamics in our model.

For $a, c > 0$, $\frac{1}{2} < b < 1$, and $\frac{b^2}{2b-1} < c^2$, system (5) undergoes a subcritical Hopf bifurcation with respect to the parameter U at the bifurcation points U_{Hopf1} and U_{Hopf2}. Moreover, there are two points $U_{SN1} < U_{Hopf1}$ and $U_{SN2} > U_{Hopf2}$ where our system has saddle node bifurcations of periodic solutions. For values $U \in [U_{SN1}, U_{Hopf1}]$ and $U \in [U_{Hopf2}, U_{SN2}]$ system (5) displays multistability. This means that there coexist a stable equilibrium, a stable periodic orbit, and an unstable periodic orbit. The interval $[U_{SN1}, U_{SN2}]$ can be regarded as the oscillation interval of the FitzHugh-Nagumo system (5).

Numerical calculations of the bifurcation scenario of Eq. (5) are shown in Fig. 1.

Working out the limit $\tau \to \infty$ in (3) defines the slow subsystem

$$\dot{U}(t) = -U(t) + qG(V(t)) + e,$$

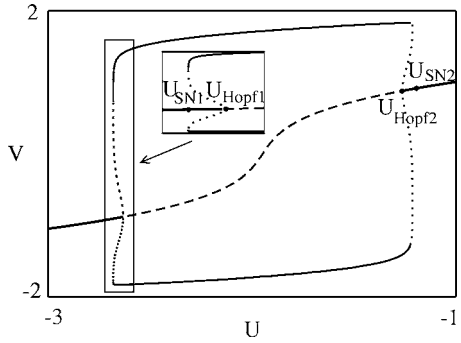

FIG. 1. Numerically computed bifurcation diagram of the FitzHugh-Nagumo system (5) with respect to the bifurcation parameter U using the software XPPAUT [19]. The bifurcation diagrams are calculated for $a=b=0.9$ and $c=2.0$. The stationary solution is drawn with bold solid lines in the stable case and with a dashed line in the unstable case. Maximal and minimal values of V for the periodic orbit are shown in the unstable case with dotted lines and in the stable case with solid lines. The insert shows the dynamics near the Hopf bifurcation point U_{Hopf1}.

$$0 = c\left(W(t) + V(t) - \frac{1}{3}V^3(t)\right) + \gamma U(t),$$

$$0 = [a - V(t) - bW(t)]/c. \tag{6}$$

From the second and third equation above we can deduce the relation

$$U = \frac{c}{\gamma}\left[\frac{1}{3}V^3 - V\left(1 - \frac{1}{b}\right) - \frac{a}{b}\right].$$

Using this and the first equation of the slow subsystem (6) we find the scalar differential equation

$$\dot{V}(t) = \frac{1}{3}\frac{[-cbV^3 - 3cV(1-b) + 3b\gamma(qG(V) + e) + 3ac]}{c(V^2 b + 1 - b)}$$

describing the dynamics of the V variable in the slow system. The last equation can have up to three stationary solutions.

The trajectories of our system (2) consist of segments for which the fast subsystem (4) is a good approximation to the dynamics and of segments for which the slow subsystem (6) is a good approximation to its dynamics. A full description of the steady state and periodic solution sets of the fast subsystem with the slow variable as a parameter and the dynamics of the slow subsystem is essentially for the understanding of the global bifurcations of the full system (2).

As it is well known, systems with slow-fast dynamics can have a burst activity which is characterized by slowly alternating phases of nearly steady-state behavior and trains of rapid spikelike oscillations. These two phases are called the silent and active phases, respectively.

Our system has only one slow variable U. In the fast subsystem we have a subcritical Hopf bifurcation for the stationary solution. The periodic orbit disappears via a saddle node bifurcation. According to the classification in [9] the burst solution of our full system is called "subHopf/fold cycle." In [4] this kind of solution is identified as "elliptic" bursting.

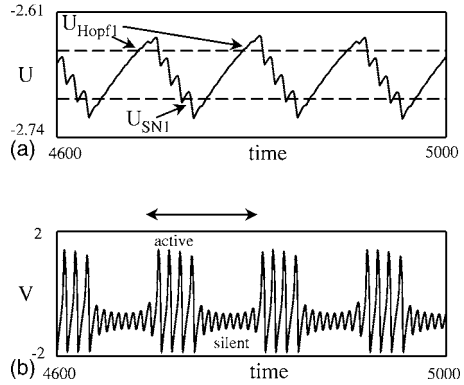

FIG. 2. Time courses of the slow variable U (a) and the fast variable V (b). Parameter values: $(a,b,c,q,\tau,\gamma)=(0.9,0.9,2,-1,100,1)$. The time interval of the slow-fast projection in Fig. 3 is indicated by the arrow.

Figures 2(a) and 2(b) show the slow variable U (a) and the fast variable V (b) depending on time. In Fig. 2(a) the horizontally dotted lines denote the Hopf bifurcation and the saddle node bifurcation of the fast subsystem. When U moves from U_{Hopf1} to U_{SN1} the system is in the active phase, and when U moves back from U_{SN1} to the next U_{Hopf1} the system is in the silent phase.

Figure 3 illustrates the active and silent phases of the systems in the slow-fast projection. The time interval of the slow-fast projection in Fig. 3 is indicated by the arrow in Fig. 2.

During the active phase U decreases toward the saddle node bifurcation U_{SN1} of the fast periodic solution. When U reaches this bifurcation point, then the trajectory falls into the domain of attraction of the stable steady state. We have then slow rightward movement along the steady-state branch during the silent phase. If U reaches the Hopf bifurcation point, the stable steady state becomes unstable and the trajectory cannot continue to track it. It returns then to the oscillation of the fast subsystem in order to initiate the active phase.

Figure 3(a) shows the fast oscillations of the system during the active phase. Note that to the left of U_{Hopf1} the at-

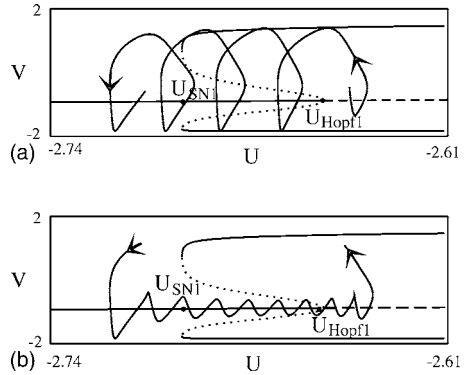

FIG. 3. Bifurcation diagram of the fast subsystem near the Hopf bifurcation point (see also the insert of Fig. 1) and projection of the solution of the full system (1) into the slow-fast (U,V) plane: (a) active phase and (b) silent phase. The values of the parameters are the same as in Fig. 2.

traction of the steady state is weak and the active phase continues "outside" the saddle node bifurcation at U_{SN1}. Figure 3(b) shows decay and growth of small oscillations during the silent phase. Moreover, when the silent phase ends, U continues to oscillate near the steady state even after U has passed the value corresponding to the Hopf bifurcation U_{Hopf1} in the fast subsystem. This phenomenon is called "slow passage effect" [9].

Thus, our system exhibits the following behavior in the phase space. In the fast subsystem we have high-frequency oscillations pushing trajectories outside the oscillation interval of the FitzHugh-Nagumo system, and in the slow direction we have attraction, which leads trajectories back to the oscillation interval and so on.

In this paper we restrict ourselves to the case of an inhibitory coupling strength ($q<0$). A bifurcation analysis for the case of excitatory coupling ($q>0$) would go beyond the scope of this paper. For the excitatory coupling parameter the slow subsystem (6) can have more than one steady state (two or three). This leads to a more complex behavior of the full system (1). The existence of the stationary solution for (1) and its stability with respect to the bifurcation parameters e and q are given in [11]. For $q>0$ it turns out that there exists also a Takens-Bogdanov bifurcation in addition to saddle node and Hopf bifurcations [13,14]. In [15] it is shown that complex dynamics arises alone in the case of two coupled network equations (without a fast subsystem).

B. Bifurcations of stationary solutions

In this section we analyze the stationary solution branch of (2) in more detail. Therefore we first summarize existing results on the stationary solutions that have been published in [11] where the delayed neuron model has been analyzed.

The stationary solution (U^*, V^*, W^*) has the form

$$U^* = qG(V^*) + e,$$

$$W^* = \frac{a - V^*}{b},$$

$$F(V^*) = 0, \tag{7}$$

with

$$F(V^*) = -\frac{c}{3}(V^*)^3 - c\left(\frac{1}{b} - 1\right)V^* + \gamma q G(V^*) + \frac{ca}{b} + \gamma e$$

and

$$F'(V^*) = -c(V^*)^2 - c\left(\frac{1}{b} - 1\right) + \gamma q G'(V^*).$$

In the case $c>0$, $1/b-1>0$, and $\gamma q<0$ the relation $F'(V^*)<0$ holds for all values a, e, τ. Hence (1) has a unique stationary solution in the form (8). In the general case system (1) can have one, two, or three stationary solutions depending on the parameter e.

A proof of the existence of the stationary solutions is given in [11]. The case of multiple stationary solutions is analyzed in more detail in [14].

Note that $F(V^*)=0$ additionally implies

$$e = \frac{1}{\gamma}\left[\frac{c}{3}(V^*)^3 + c\left(\frac{1}{b} - 1\right)V^* - \gamma q G(V^*) - \frac{ac}{b}\right]. \tag{8}$$

Linearizing Eq. (2) along the stationary solution (U^*, V^*, W^*) yields

$$\dot{U}(t) = \frac{1}{\tau}[-U(t) + qG'(V^*)V(t)],$$

$$\dot{V}(t) = c\{W(t) + [1 - (V^*)^2]V(t)\} + \gamma U(t),$$

$$\dot{W}(t) = [-V(t) - bW(t)]/c. \tag{9}$$

The matrix of the linearized system (9) has the characteristic polynomial

$$p(\lambda) = -\lambda^3 + Q_1\lambda^2 + Q_2\lambda + Q_3 \tag{10}$$

with

$$Q_1 = c[1 - (V^*)^2] - \left(\frac{b}{c} + \frac{1}{\tau}\right),$$

$$Q_2 = c[1 - (V^*)^2]\left(\frac{b}{c} + \frac{1}{\tau}\right) - \frac{b}{c\tau} - 1 + \gamma\frac{q}{\tau}G'(V^*),$$

$$Q_3 = \frac{b}{\tau}[1 - (V^*)^2] - \frac{1}{\tau} + \frac{b\gamma q}{c\tau}G'(V^*).$$

At a parameter value that corresponds to a Hopf bifurcation equation $p(\lambda)=0$ possesses one root $\lambda_1 \in \mathbb{R}$ and two pure imaginary roots $\lambda_2 = i\beta$, $\lambda_3 = -i\beta$, $\beta \neq 0$. Thus the equation $p(\lambda)=0$ has the form

$$\lambda^3 - \lambda_1\lambda^2 + \beta^2\lambda - \lambda_1\beta^2 = 0.$$

So we obtain the conditions for the Hopf bifurcation,

$$\lambda_1 = Q_1, \quad \beta^2 = -Q_2, \quad \lambda_1\beta^2 = Q_3, \tag{11}$$

or, in a more simple form, $Q_1Q_2 + Q_3 = 0$.

Returning to our original parameters yields

$$K^2 m - K(m^2 + 1) + KD - \frac{1}{\tau}D + \frac{b}{c}\left(1 + \frac{m}{\tau}\right) = 0 \tag{12}$$

with the abbreviations

$$K = c[1 - (V^*)^2], \quad D = \frac{\gamma q}{\tau}G'(V^*), \quad m = \frac{b}{c} + \frac{1}{\tau}.$$

Note that $\lambda_1<0$ holds in our parameter setting. So the solutions of (12) determine the Hopf bifurcation in (2). From (8) we obtain the corresponding parameter values e_{Hopf1} and e_{Hopf2}. In order to show an example of the occurring bifurcations of system (1) we fix the parameters to $(a, b, c, \gamma, q, \tau) = (0.9, 0.9, 2.0, 1.0, -1.0, 100)$ and compute numerically the bifurcation diagram with respect to the parameter e. In the chosen parameter case the fast subsystem has only one stationary solution and the slow subsystem has a unique asymptotically stable equilibrium. Figure 4 shows

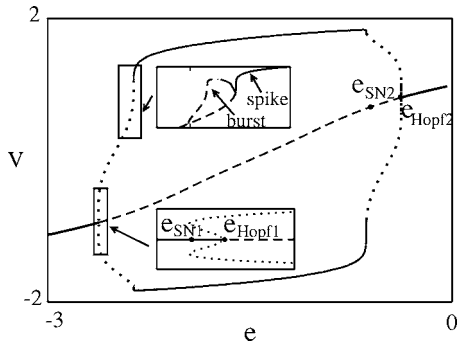

FIG. 4. Numerically calculated bifurcation diagram of system (1) with respect to the parameter e using XPPAUT [19]. Bold black lines denote stable stationary solutions and black dashed lines represent unstable stationary solutions. The maximal and minimal values of V for the stable periodic orbits are drawn with solid black lines and with dotted lines for unstable periodic orbits. The inserts show the dynamics near the Hopf bifurcation point e_{Hopf1} (bottom) and interval for burst solution (top).

the numerically calculated bifurcation diagram for the parameter e. There are values e_{Hopf1} and e_{Hopf2} such that for all e in the interval $e<e_{Hopf1} \cup e>e_{Hopf2}$ system (1) has a stable stationary solution in the form (8). Moreover, the conditions (12) and (8) define Hopf bifurcations which appear subcritical due to the results of the numerically calculated bifurcations (see Fig. 4, bottom insert). Before the occurrence of the Hopf bifurcation the system has a saddle node bifurcation of periodic orbits (see Fig. 4, lower insert). As a result, we obtain two unstable periodic solutions. One of them goes to the stationary solution and disappears at the Hopf bifurcation point. The other branch of unstable periodic solutions bifurcates into the stable spikelike solutions (see Fig. 4, upper insert).

III. NUMERICAL SIMULATIONS

This chapter provides numerical simulations of our neuron system in order to show its dependence on the two important bifurcation parameters e (external signal) and τ (synaptic time constant). The simulations clarify which types of dynamics can occur for special parameter sets. In addition, the stability of the different types of oscillations is determined.

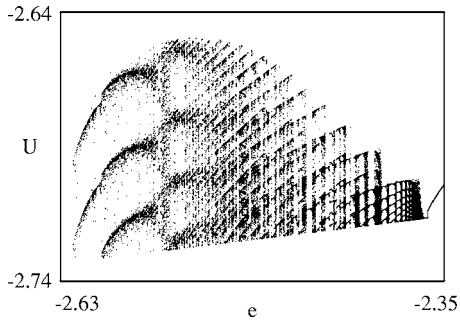

FIG. 5. U components of the intersections of trajectories with the Poincaré section $U+V+4.3=0$.

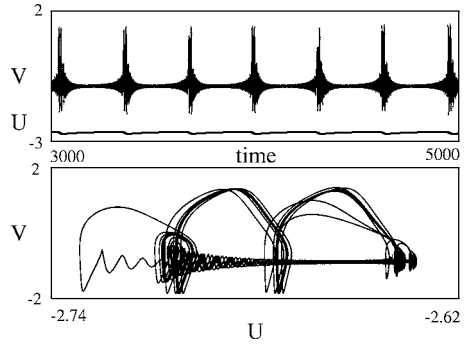

FIG. 6. Numerical simulation of the neuron system (1) for $e_1=-2.6$. Top: $V(t)$ (upper curve) and $U(t)$ (lower curve) displaying a chaotic burst solution. Bottom: Projection into the slow-fast (U,V) plane.

A. e as bifurcation parameter

In this section we analyze the bifurcation scenario with respect to the parameter e in more detail.

Directly after the subcritical Hopf bifurcation our system does not have a stable periodic orbit. The solutions of our system in this interval (after the Hopf bifurcation and before the appearance of the spikelike solutions) have a characteristic burstlike form. Moreover, we obtain windows of periodic and chaotic motion with respect to the parameter e. To classify these burstlike solutions we use the Poincaré section techniques. A close look at Figs. 6–9 shows that hypersurfaces of the form $U+V\approx-4$ seem to be of interest. For our actual computations we have chosen the hypersurface $U+V+4.3=0$. In Fig. 5 the U component (slow variable) of the Poincaré section with respect to the parameter e is shown. We use the parameter values as $(a,b,c,q,\gamma,\tau)=(0.9,0.9,2.0,-1.0,1.0,100.0)$. As we can see, we have windows with regular (stable periodic orbits) and chaotic motions.

As a snapshot we present some computations for the system (2) at four different values: $e_1=-2.6$, $e_2=-2.5$, $e_3=-2.38$, and $e_4=-2.35$. In all of our examples we use $(a,b,c,q,\gamma,\tau)=(0.9,0.9,2.0,-1.0,1.0,100.0)$. In Figs. 6–9 the U and V components are plotted versus time and a projection of the solution into the "slow-fast" plane (U,V) is

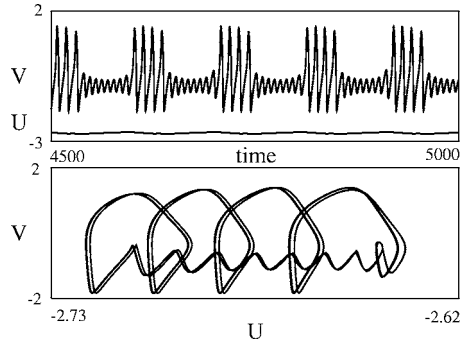

FIG. 7. Numerical simulation of the neuron system (1) for $e_2=-2.5$. Top: $V(t)$ (upper curve) and $U(t)$ (lower curve) displaying a stable periodic burst solution. Bottom: Projection into the slow-fast (U,V) plane.

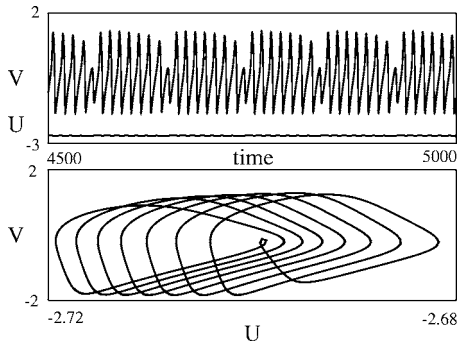

FIG. 8. Numerical simulation of the neuron system (1) for $e_3=-2.38$. Top: $V(t)$ (upper curve) and $U(t)$ (lower curve) displaying a stable periodic solution which is a transition between bursting and spiking. Bottom: Projection into the slow-fast (U,V) plane.

shown. To clarify the structure of the dynamics on these sets we compute the corresponding Lyapunov exponents λ (see, e.g., [20] for a definition). We have to compute three exponents, one of them always being equal to zero, corresponding to the tangential direction of the flow, and the remaining two determine the structure and the stability of these sets. Figures 10(a)–10(d) show the two maximal Lyapunov exponents for the invariant set to the corresponding values of e_i, $i=1,\ldots,4$.

For $e=e_1=-2.6$ (see Fig. 6) we have a chaotic burst solution. $V(t)$ displays the classical form of a burst and the maximal Lyapunov exponent [Fig. 10(a)] is positive ($\lambda_{max}\approx 0.005$).

In the case $e=e_2=-2.5$ (Fig. 7) we observe a stable periodic burst trajectory. This follows from the fact that the maximal Lyapunov exponent is 0, but the second one is negative. Figure 10(b) shows $\lambda\approx -0.001$.

For $e=e_3=-2.38$, Fig. 8 shows a stable periodic solution which is a transition-type between burst and spike solutions. The second maximal Lyapunov exponent is negative [$\lambda=-0.02$ in Fig. 10(c)].

Finally, in the case $e=e_4=-2.35$ (Fig. 9) we obtain a spiking periodic solution. The maximal exponent is 0, and the second one is negative [see Fig. 10(d)].

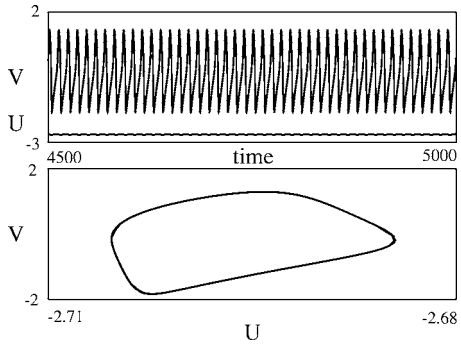

FIG. 9. Numerical simulation of the neuron system (1) for $e_4=-2.35$. Top: $V(t)$ (upper curve) and $U(t)$ (lower curve) displaying a stable periodic solution in the form of spiking. Bottom: Projection into the slow-fast (U,V) plane.

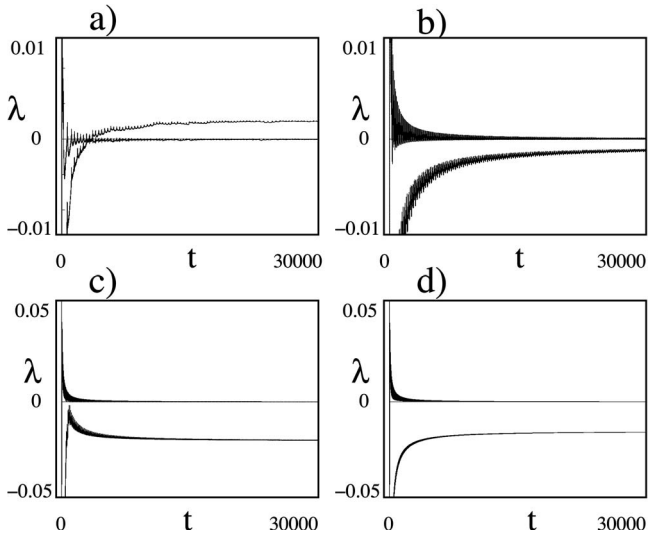

FIG. 10. Two maximal Lyapunov exponents λ of the neuron system. Lyapunov exponents for (a) $e_1=-2.6$, (b) $e_2=-2.5$, (c) $e_3=-2.38$, and (d) $e_4=-2.35$.

B. τ as bifurcation parameter

In this section we analyze the bifurcations of the system (1) with respect to the parameter τ. The remaining parameters are fixed at the same values ($a=0.9$, $b=0.9$, $c=2.0$, $\gamma=1.0$, $q=-1.0$) as in the last section, and we choose $e=-2.5$. For a classification of the different nontrivial solutions we use Poincaré section techniques. An interesting hypersurface turns out to be the cut $U+V+4.3=0$ through the phase space. In Fig. 11 the V components of the intersections of interesting trajectories with the Poincaré section are shown. Depending on the actual value of τ, our system has stable periodic and complex burst chaotic solutions.

The corresponding solutions to the values $\tau_1=60$, $\tau_2=160$, and $\tau_3=67$ are plotted in Figs. 12 and 13. As these diagrams show, our system has periodic and chaotic solutions. Moreover, multistable phenomena can also take place. For $\tau_1=60$ we obtain a stable periodic burst solution [Fig. 12(a)], for $\tau_2=160$ we have a chaotic burst solution [Fig. 12(b)], and in the case $\tau_3=67$ there is a coexistence of a stable periodic and chaotic burst solution (see Fig. 13). Figure 14 shows the two maximal exponents for (a) the periodic solution from Fig. 13 and (b) the chaotic solution from Fig. 13.

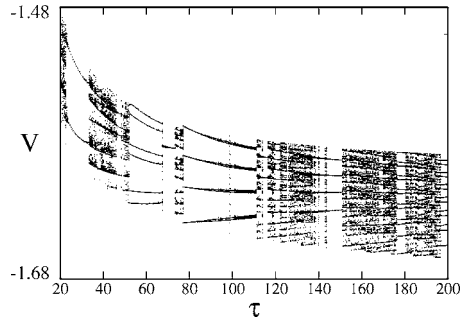

FIG. 11. V components of the intersections of trajectories with the Poincaré section $U+V+4.3=0$.

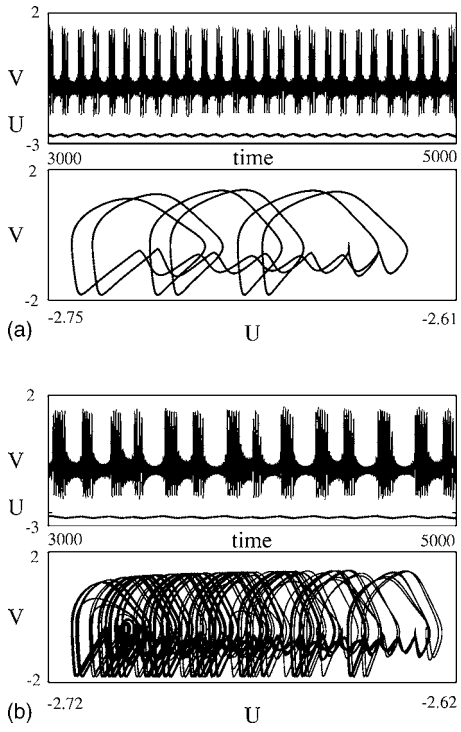

FIG. 12. Numerical simulation of the neuron system (1) for (a) $\tau_1=60$ and (b) $\tau_2=160$. Top: $V(t)$ (upper curve) and $U(t)$ (lower curve) displaying (a) a periodic burst solution and (b) a chaotic burst solution. Bottom: Projection into the slow-fast (U,V) plane.

For an explanation ansatz of this bifurcation scenario we compute the Poincaré section on the surface $U+V+4.3=0$ and display the result in the (U,W) plane (see Fig. 15). An important observation of Fig. 15 with fixed τ is now there is a functional relation of the form $U=K(W)$. This is demonstrated in the (U,W) coordinates for different values of τ, namely, $\tau=100$, $\tau=160$, and $\tau=200$ (see Fig. 15). A consequence of that fact is that the Poincaré dynamics with fixed τ is guided by a one-dimensional map. In order to discover the underlying function of that 1D map, we plot U values of consecutive iterates in the $(U(n),U(n+1))$ plane for $\tau=100$, $\tau=160$, and $\tau=200$ (see Fig. 16).

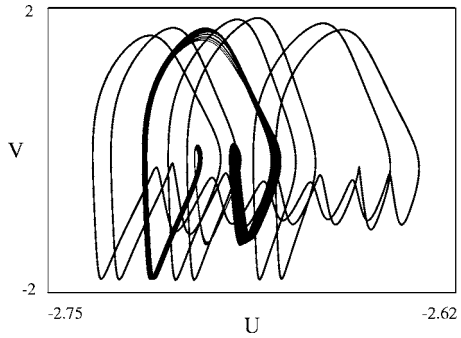

FIG. 13. Numerical simulation of the neuron system (1) for $\tau_3=67$. Coexistence of a stable periodic and a chaotic burst solution. Projection into the slow-fast (U,V) plane.

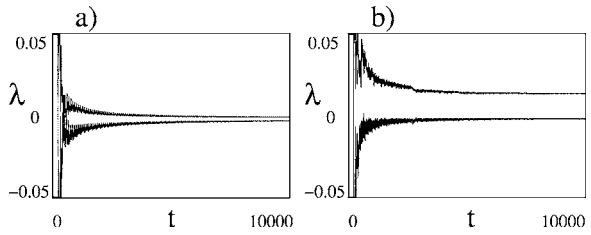

FIG. 14. Two maximal Lyapunov exponents. Left: Lyapunov exponents for the periodic burst solution corresponding to $\tau_3=67$. Right: Lyapunov exponents for the chaotic burst solution corresponding to $\tau_3=67$.

IV. ANALYSIS OF THE BIFURCATED NONSTATIONARY SOLUTIONS

In this section we analyze the dynamical features of the attractors appearing on the τ-solution branch. Our starting point is the analysis of the computed Poincaré map (see Fig. 16). The first step is to normalize the map shown in Fig. 16 into $[0,1]\times[0,1]$ and to find an approximation for the generating function. Our fitting ansatz is a linear function for the right part and a hyperbolic function of the form $a+b/(c*x+d)$ for the left part. This leads to the iteration

$$x_{n+1}=f_{p,q,k,l}(x_n) \tag{13}$$

with the generator function

$$f_{p,q,k,l}(x)=\begin{cases}\dfrac{p}{qk}\left(-1+\dfrac{qk+p}{qx+p}\right), & x<k\\ l(x-k), & x\geqslant k\end{cases} \tag{14}$$

and p,q,k,l in the set

$$P=\{(p,q,k,l)\in\mathbb{R}^4: p<0, q<-p/k\ ,$$

$$k\in(0,1), 0<l<1/(1-k)\}.$$

The fitting results for certain values of τ are shown in Fig. 17.

Figure 17 shows that there is a good coincidence between the numerically computed maps Fig. 16 and with its approximations. We can deduce the following relations from Fig. 17.

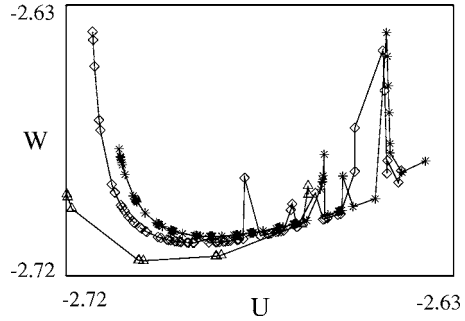

FIG. 15. Poincaré dynamics shown in the (U,W) plane. The orbit for $\tau=100$ is denoted with triangles, for $\tau=160$ with diamonds, and for $\tau=200$ with stars.

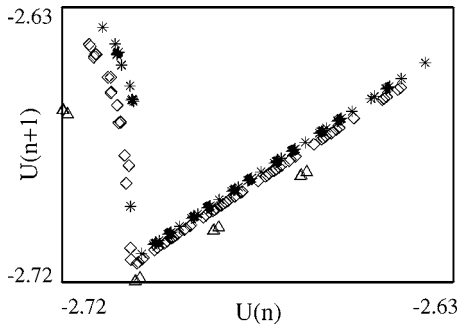

FIG. 16. Poincaré map for $\tau=100$ (triangles), $\tau=160$ (diamonds), and $\tau=200$ (stars).

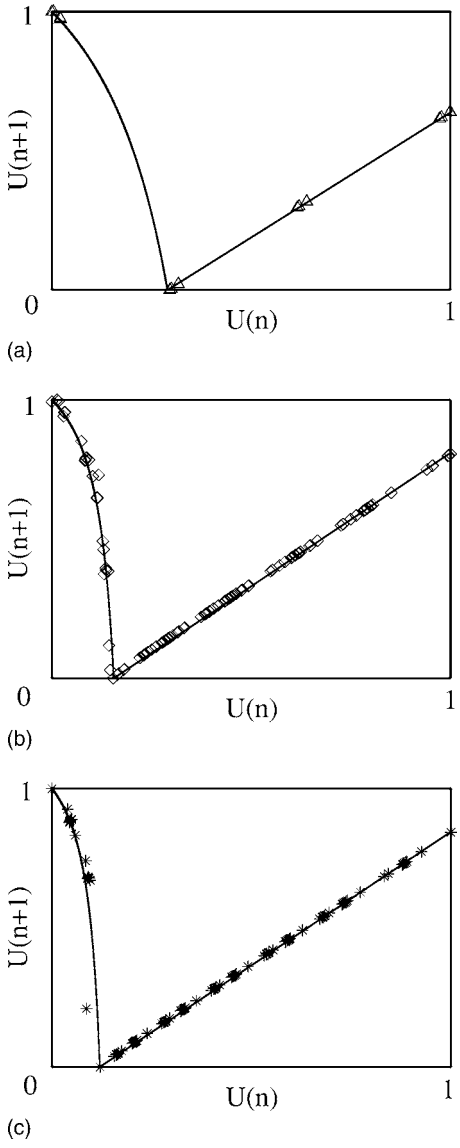

FIG. 17. Approximations (14) of the 1D Poincaré map: (a) $\tau=100$: $p_1=-1$, $q_1=2$, $k_1=0.29$, $l_1=0.9$; (b) $\tau=160$: $p_2=-1$, $q_2=5$, $k_2=0.155$, $l_2=0.96$; and (c) $\tau=200$: $p_3=-1$, $q_3=6.5$, $k_3=0.12$, $l_3=0.965$.

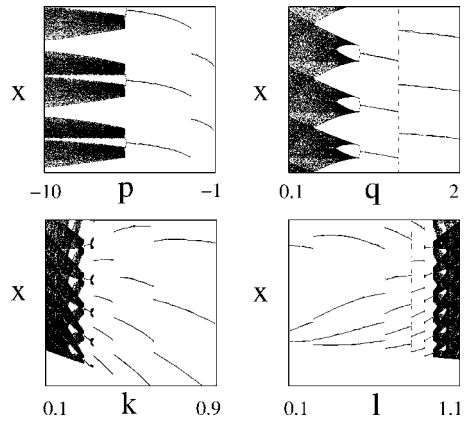

FIG. 18. Analytical approximation of the 1D Poincaré map. Bifurcation diagrams of the map for the four parameters p, q, k, l of the approximation.

An increase of τ corresponds to an increase of q and a decrease of k. The value of l seems to act nearly independent of τ.

Next we analyze the iterative process Eqs. (13) and (14). Obviously, the interval $[0, 1]$ is invariant for the map. Moreover, the dynamics of Eqs. (13) and (14) has always exactly one fixed point in $[0,1]$, namely

$$x^* = \{-p(1+k) - \sqrt{[p(1+k)]^2 + 4pqk^2}\}/(2qk)$$

which is unstable.

The most important point is to characterize the nonstationary long time behavior of Eq. (13). For parameter values $w=(p,q,k,l)$ in

$$\hat{P} := \{(p,q,k,l) \in P; k < l(1-k), k < l[l(1-k)-k]\},$$

we can easily calculate

$$f_w(0) = 1,$$

$$f_w^2(0) = f_w(1) = l(f_w(0) - k) \in (k, f_w(0)),$$

$$f_w^3(0) = f_w^2(1) = l(f_w^2(0) - k) \in (k, f_w^2(0)),$$

$$f_w^4(0) = f_w^3(1) = l(f_w^3(0) - k) \in (0, f_w^3(0)).$$

The intermediate value theorem applied to the continuous function $f^3_{p,q,k,l}:[0,1]\to[0,1]$ proves the existence of a period three orbit for $f_w=f_{p,q,k,l}$, $(p,q,k,l) \in \hat{P}$. The famous theorem of Li and Yorke [21] ensures that there are periodic orbits of every period $n \in \mathbb{N}$ and an uncountable subset S of $[0,1]$ containing no asymptotically periodic points in the dynamics (13).

Thus, for $w=(p,q,k,l) \in \hat{P}$ including our parameter sets $p_i, q_i, k_i l_i$, $i=1,2,3$ we have shown the existence of the so called Li-Yorke chaos in the dynamics of (13). Since the Li-Yorke chaos takes place in a Poincaré cut of (1), this means that the attractor of the original system contains periodic orbits of arbitrary length and an uncountable set of orbits with asymptotically periodic behavior. These results are an impressive theoretical confirmation for the computed cha-

otic invariant sets in Sec. III B. The presented analysis admits precise insights into the internal structure of the attractor which cannot be obtained by purely numerical computations.

In order to obtain information about the bifurcation scenario in the complement area of $\hat{P}$ in the parameter space, we complete this section by simulating the dynamics of (13) with respect to each of the parameter of $f_{p,q,k,l}$ and present four different one-dimensional (1D) map bifurcation diagrams (see Fig. 18).

Each of the pictures in Fig. 18 shows that the map (14) with respect to the corresponding bifurcation parameter undergoes a lot of bifurcation phenomena. We have windows showing periodic cycles and chaotic motion. More precisely, in the chaotic regions (black regions in Fig. 18) we observe the appearance of periodic orbits of arbitrary order and the existence of a dense orbit for the discrete dynamics (13). This means that for the original system (1) we have ensured the existence of periodic orbits wriggling up arbitrarily, often around a base orbit, and chaotic sets having the shape of a blown up, closed curve in our original dynamical system. The invariant sets plotted in Figs. 12 and 13 are exactly of this type.

V. CONCLUSIONS

This paper provides a characterization into interesting dynamical properties of a single neuron model. The behavior of the system with respect to important bifurcation parameters was analyzed. It turns out that the system possesses a rich structure of different oscillatory dynamics. The two oscillation types, bursting and spiking, were investigated with respect to their stability using Lyapunov exponents. We found that there exist chaotic burst solutions, stable periodic burst solutions, stable transition states between bursting and spiking, as well as stable spike solutions. This was done by theoretical investigation of a one-dimensional Poincaré map with the Li and Yorke theorem.

Moreover, the present paper contains a numerically obtained overview of some dynamical properties of our neuron model completed by some analytical examinations. Nevertheless, there are some remaining problems. The analytical proof of the existence of Hopf bifurcations in the neuron model without delay is one of the future plans of the authors, as well as the detailed description of the bifurcation mechanisms and the interactions of slow and fast dynamics that lead to bursting and spiking in this model.

ACKNOWLEDGMENT

We are very grateful to Fotios Giannakopoulos for many discussions and valuable suggestions.

[1] A. L. Hodgkin and A. F. Huxley, J. Physiol. (London) **117**, 500 (1952).
[2] F. Giannakopoulos, U. Bihler, C. Hauptmann, and H. J. Luhmann, Biol. Cybern. **85**, 257 (2001).
[3] T. R. Chay and J. Keizer, Biophys. J. **42**, 181 (1983).
[4] J. Rinzel, Lect. Notes Biomath. **71**, 267 (1987).
[5] R. FitzHugh, J. Gen. Physiol. **43**, 867 (1960).
[6] R. FitzHugh, Biophys. J. **1**, 445 (1961).
[7] J. Nagumo, S. Arimoto, and S. Yoshizava, Proc. IRE **50**, 2061 (1962).
[8] R. E. Plant, SIAM J. Appl. Math. **40**, 151 (1981).
[9] E. M. Izhikevich, Int. J. Bifurcation Chaos Appl. Sci. Eng. **10**, 1171 (2000).
[10] E. M. Izhikevich, SIAM J. Appl. Math. **60**, 503 (2000).
[11] F. Giannakopoulos, C. Hauptmann, and A. Zapp, Fields Inst. Commun. **29**, 147 (2001).
[12] Ch. Hauptmann, Ph.D Thesis, University of Cologne, Germany (2000).
[13] A. Gail, Ph.D Thesis, University of Cologne, Germany (2004).
[14] A. Gail and F. Giannakopoulos (unpublished).
[15] F. Giannakopolous and O. Oster, Differential Equations and Dynamical Systems **5**, 229 (1997).
[16] E. Kaumann and U. Staude, Lect. Notes Math. **1017**, 313 (1983).
[17] I. Hsü and N. D. Kazarinoff, J. Math. Anal. Appl. **55**, 61 (1976).
[18] K. P. Hadeler, U. an der Heiden, and K. Schumacher, Biol. Cybern. **23**, 211 (1976).
[19] B. Ermentrout, *XPPAUT 5.5—The Differential Equations Tool* (download of the program from http://www.math.pitt.edu/bard/xpp/download.html).
[20] A. Wolf, J. Swift, H. L. Swinney, and A. Vastano, Physica D **16**, 285 (1985).
[21] T. V. Li and J. A. Yorke, Am. Math. Monthly **82**, 985 (1975).